AIP | Journal of Applied Physics

Temporal coupled mode theory linking to surface-wave dispersion relations in near-field electromagnetic heat transfer

Hideo Iizuka and Shanhui Fan

Citation: Journal of Applied Physics **120**, 194301 (2016); doi: 10.1063/1.4967832
View online: http://dx.doi.org/10.1063/1.4967832
View Table of Contents: http://scitation.aip.org/content/aip/journal/jap/120/19?ver=pdfcov
Published by the AIP Publishing

Temporal coupled mode theory linking to surface-wave dispersion relations in near-field electromagnetic heat transfer

Hideo Iizuka[1,a)] and Shanhui Fan[2,b)]
[1]*Toyota Central Research & Development Labs., Nagakute, Aichi 480 1192, Japan*
[2]*Department of Electrical Engineering, Ginzton Laboratory, Stanford University, Stanford, California 94305, USA*

(Received 14 September 2016; accepted 3 November 2016; published online 16 November 2016)

We provide a detailed discussion of the use of coupled mode theory to describe near-field heat transfer. We consider a simple physical model system of coupled harmonic oscillators with each oscillator maintaining at a different temperature, where heat transfer between the oscillators can be analytically treated from first-principles using the Newton's equation and the fluctuation dissipation theorem. Applying a slowly varying envelope approximation to the Newton's equation, we derive a coupled mode theory formalism. We then apply this coupled mode theory formalism in the study of the near-field heat transfer between either silicon carbide plates or between two graphene sheets. The coupled mode theory provides a quantitative link between the dispersion relation of the coupled system and the heat transfer, and agrees with exact numerical results over all range of wavevectors. To obtain such complete agreement, the key observation here is that one should include the frequency shift, that is, the frequency of the individual mode used in the coupled mode theory should be different from the frequency of the mode of an isolated structure. Finally, we show that the coupled mode theory can be applied even when more than two modes are involved in the heat transfer. As an example, we extend our formalism to the near-field heat transfer in a four-layer graphene structure. *Published by AIP Publishing.*
[http://dx.doi.org/10.1063/1.4967832]

I. INTRODUCTION

Near-field heat transfer is of great importance for heat management in the nanoscale, since it significantly exceeds the far-field limit.[1–13] While most early previous works focused on numerical studies,[14–28] there have been significant recent works seeking to develop analytic upper bound of near-field heat transfer.[29–35]

Complementary to numerical works, a practically powerful approach to generate analytic insights is through the use of coupled mode theory.[36–41] Since in many prominent geometries for the study of near-field heat transfer, the dominant contributions arise from the surface polaritons, it is natural to seek to describe the heat transfer from the properties of these modes. Hence a number of authors have applied coupled mode theory for heat transfer.[42,43] Both Otey and Chalabi have shown that the coupled mode theory agrees very well with exact calculation in the quasi-static regime, where the wavevector of the polariton is much larger compared with the free-space wavevector. Outside the quasi-static regime, however, Chalabi has noted that there is discrepancy between their coupled mode theory approach and exact results.[43]

In this paper, we show that a simple modification of the formalism used in Refs. 42 and 43 leads to complete agreement between the coupled mode theory and the exact numerical results over all range of wavevectors. The key observation here is that one should not use the polariton frequency of a single interface as the modal frequency in the coupled mode theory; instead, one should include the frequency shift as induced by the second interface. We show that the modified coupled mode theory excellently reproduces the exact numerical results in different material systems including silicon carbide (SiC) and graphene. The existence of such frequency shift is certainly well known in photonics[38] and has been previously observed in several theoretical studies on near-field heat transfer between material bodies.[15,44,45] However, there have not been any previous works highlighting the importance of incorporating such a frequency shift in the temporal coupled mode theory formalism for describing near-field heat transfer. In addition, we verify the applicability of the theory for a four-layer graphene structure. Therefore, we have shown that the properties of the near-field heat transfer can be completely and quantitatively understood in terms of the property of the underlying electromagnetic modes. This should enable one to design the properties of electromagnetic modes for the purpose of controlling heat transfer.

The paper is organized as follows. In Section II, we develop a coupled mode theory by using a harmonic oscillator model and introducing a slowly varying envelope approximation. In Section III, we compare the coupled mode theory formalism to numerical results in the heat transfer per channel and obtain excellent agreements. In addition, we extend our formalism to the near-field heat transfer in a four-layer graphene structure and clarify the frequency shifts occurring in the coupled system. The paper is then concluded in Section IV.

[a)]hiizuka@mosk.tytlabs.co.jp
[b)]shanhui@stanford.edu

II. COMPARISON OF COUPLED MODE THEORY WITH A SIMPLE PHYSICAL MODEL

Given the discrepancy observed between the coupled mode theory and the actual numerical results in Ref. 43, we seek to reexamine the foundation of such coupled mode theory formalism. In Section II A, we consider a simple physical model system of coupled harmonic oscillators with each oscillator maintaining at a different temperature, where heat transfer between the oscillators can be analytically treated from first-principles using the Newton's equation and the fluctuation dissipation theorem. The equation here involves a second-order derivative in time. In Section II B, we then derive a coupled mode theory, which involves a first-order derivative in time, for the same system shown in Section II A, applying a slowly varying envelope approximation to the Newton's equation. This derivation shows that the standard coupled mode theory formalism for heat transfer, at least for this simple system, can be derived from first-principles. The derivation also provides important insights into the correct choice of the coupled mode theory parameters that are required in order to quantitatively describe the physical model system.

A. Heat transfer between two harmonic oscillators

We consider heat transfer between two harmonic oscillators, and each as shown in Fig. 1(a), is described by

$$\frac{d^2x}{dt^2}+\gamma\frac{dx}{dt}+\omega_s^2x=\frac{F}{m}, \tag{1}$$

where x is the oscillating amplitude, γ is the damping rate, ω_s is the resonant frequency, F is an external force that acts on the oscillator, and m is the mass of the oscillator. The resonant frequency has the form of $\omega_s=\sqrt{\kappa_s/m}$, where κ_s is the spring constant. We assume the $\exp(-i\omega t)$ convention.

The total energy E in the harmonic oscillator, averaged over a period, is

$$E=2\cdot\frac{1}{2}Re\left[\frac{1}{2}m\omega_s^2|x|^2\right]=\frac{1}{2}m\omega_s^2|x|^2. \tag{2}$$

Here, we have switched to the phasor (i.e., complex field) notation, and notice that the total energy is twice the time-average of the potential energy. At thermal equilibrium, we should have

$$\left\langle\frac{1}{2}m\omega_s^2|x|^2\right\rangle=\Theta(\omega_s,T), \tag{3}$$

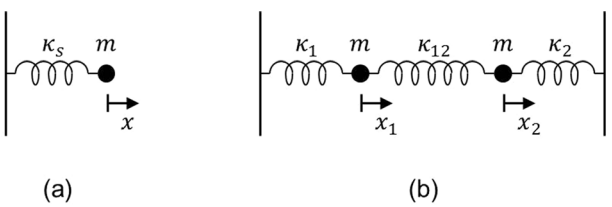

FIG. 1. Analytic models of (a) a single harmonic oscillator and (b) two-coupled harmonic oscillators.

where

$$\Theta(\omega_s,T)=\frac{\hbar\omega_s}{e^{\frac{\hbar\omega_s}{k_BT}}-1}, \tag{4}$$

$\hbar$ and k_B are the reduced Planck constant and the Boltzmann constant, respectively. In general, when $F=0$, Eq. (1) describes a damped oscillator. Therefore, in order to use Eq. (1) to describe an oscillator in thermal equilibrium, the right hand side of Eq. (1) should be a fluctuating force that compensates for the damping. In the frequency domain, Eq. (1) becomes

$$x(\omega)=\frac{F(\omega)}{m}\frac{1}{\omega_s^2-\omega^2-i\omega\gamma}. \tag{5}$$

Therefore

$$\begin{aligned}\langle|x|^2\rangle&=\int_{-\infty}^{\infty}\frac{d\omega}{2\pi}\int_{-\infty}^{\infty}\frac{d\omega'}{2\pi}e^{-i(\omega-\omega')t}\langle x(\omega)x^*(\omega')\rangle\\&=\frac{1}{m^2}\int_{-\infty}^{\infty}\frac{d\omega}{(2\pi)^2}\frac{F(\omega)}{\left(\omega_s^2-\omega^2\right)^2+\omega^2\gamma^2},\end{aligned} \tag{6}$$

where we have assumed that the fluctuating force is also stationary, that is, $\langle|F(t)|^2\rangle$ is time-independent, and thus

$$\langle F(\omega)F^*(\omega')\rangle=F(\omega)\delta(\omega-\omega'). \tag{7}$$

Assuming that the fluctuating force is sufficiently broadband, $F(\omega)$ can be approximated as $F(\omega_s)$ and taken out of the integral. Evaluating the integral in Eq. (6), we have

$$\langle|x|^2\rangle=\frac{F(\omega_s)}{4\pi\gamma m^2\omega_s^2}. \tag{8}$$

Therefore, combining with Eq. (3), we obtain

$$F(\omega_s)=8\pi m\gamma\Theta(\omega_s,T). \tag{9}$$

Since ω_s can be chosen to be of any value in this derivation, we have

$$F(\omega)=8\pi m\gamma\Theta(\omega,T). \tag{10}$$

To summarize the derivation process of Eqs. (1)–(10), a single harmonic oscillator in thermal equilibrium is described by Eq. (1) where the fluctuating force F has the form

$$F=\int_{-\infty}^{\infty}\frac{d\omega}{2\pi}F(\omega)e^{-i\omega t}, \tag{11}$$

with

$$\langle F(\omega)F^*(\omega')\rangle=8\pi m\gamma\Theta(\omega,T)\delta(\omega-\omega'). \tag{12}$$

We next consider two harmonic oscillators coupled together, as shown in Fig. 1(b). The equations of motion are given by

$$\begin{aligned}&\frac{d^2}{dt^2}\begin{pmatrix}x_1\\x_2\end{pmatrix}+\gamma\frac{d}{dt}\begin{pmatrix}x_1\\x_2\end{pmatrix}+\frac{1}{m}\begin{pmatrix}\kappa_1+\kappa_{12}&-\kappa_{12}\\-\kappa_{12}&\kappa_2+\kappa_{12}\end{pmatrix}\begin{pmatrix}x_1\\x_2\end{pmatrix}\\&=\frac{1}{m}\begin{pmatrix}F_1\\F_2\end{pmatrix},\end{aligned} \tag{13}$$

where κ_1 and κ_2 represent the spring constants for each oscillator. Here we assume $\kappa_1 = \kappa_2 = \kappa$. κ_{12} describes the strength of coupling between the two oscillators. In the frequency domain, from Eq. (13) we have

$$\begin{pmatrix} -\omega^2 - i\gamma\omega + \frac{\kappa+\kappa_{12}}{m} & -\frac{\kappa_{12}}{m} \\ -\frac{\kappa_{12}}{m} & -\omega^2 - i\gamma\omega + \frac{\kappa+\kappa_{12}}{m} \end{pmatrix} \begin{pmatrix} x_1(\omega) \\ x_2(\omega) \end{pmatrix} = \frac{1}{m} \begin{pmatrix} F_1(\omega) \\ F_2(\omega) \end{pmatrix}. \tag{14}$$

For the lossless case ($\gamma = 0$), resonant frequencies of the coupled system are

$$\omega_H = \sqrt{\frac{\kappa + 2\kappa_{12}}{m}}, \tag{15}$$

$$\omega_L = \sqrt{\frac{\kappa}{m}}. \tag{16}$$

Using Eqs. (15) and (16), Eq. (13) is rewritten as

$$\frac{d^2}{dt^2}\begin{pmatrix} x_1 \\ x_2 \end{pmatrix} + \gamma\frac{d}{dt}\begin{pmatrix} x_1 \\ x_2 \end{pmatrix} + \begin{pmatrix} \frac{\omega_H^2+\omega_L^2}{2} & -\frac{\omega_H^2-\omega_L^2}{2} \\ -\frac{\omega_H^2-\omega_L^2}{2} & \frac{\omega_H^2+\omega_L^2}{2} \end{pmatrix} \begin{pmatrix} x_1 \\ x_2 \end{pmatrix} = \frac{1}{m}\begin{pmatrix} F_1 \\ F_2 \end{pmatrix}. \tag{17}$$

We emphasize in Eq. (17) that the behavior of the coupled oscillators is now characterized by the two resonant frequencies ω_H and ω_L of the coupled system.

In the frequency domain, from Eq. (17) we have

$$\begin{pmatrix} x_1(\omega) \\ x_2(\omega) \end{pmatrix} = \frac{1}{m\left\{\left(\frac{\omega_H^2+\omega_L^2}{2} - \omega^2 - i\gamma\omega\right)^2 - \left(\frac{\omega_H^2-\omega_L^2}{2}\right)^2\right\}} \times \begin{pmatrix} \frac{\omega_H^2+\omega_L^2}{2} - \omega^2 - i\gamma\omega & \frac{\omega_H^2-\omega_L^2}{2} \\ \frac{\omega_H^2-\omega_L^2}{2} & \frac{\omega_H^2+\omega_L^2}{2} - \omega^2 - i\gamma\omega \end{pmatrix} \begin{pmatrix} F_1(\omega) \\ F_2(\omega) \end{pmatrix}. \tag{18}$$

We now treat the heat transfer between the two oscillators, when the two oscillators are maintained at temperatures T_1 and T_2, respectively. From Eqs. (7), (10), and (18), the power transfer $P_{1\to2}$ can be determined as

$$\begin{aligned} P_{1\to2} &= Re\left[\left\langle F_{1\to2}^* \frac{dx_2}{dt}\right\rangle\right] \\ &= \frac{1}{2} Im\left[m\frac{\omega_H^2-\omega_L^2}{2}\int_{-\infty}^{\infty}\frac{d\omega}{2\pi}\int_{-\infty}^{\infty}\frac{d\omega'}{2\pi}e^{-i(\omega-\omega')t}\omega\langle x_1^*(\omega')x_2(\omega)\rangle\right] \\ &= \int_0^{\infty}\frac{d\omega}{2\pi}\frac{4\left(\frac{\omega_H^2-\omega_L^2}{2}\right)^2\gamma^2\omega^2[\Theta(\omega,T_1)-\Theta(\omega,T_2)]}{\left|\left[\left(\omega^2 - \frac{\omega_H^2+\omega_L^2}{2}\right) + i\gamma\omega\right]^2 - \left(\frac{\omega_H^2-\omega_L^2}{2}\right)^2\right|^2}, \end{aligned} \tag{19}$$

where in the first line above, we have related the transferred power to the force $F_{1\to2} = \kappa_{12}(x_1 - x_2)$ on the oscillator 2 from the oscillator 1. In the second line, the period-averaged transferred power has been given by using $Re[\langle F_{1\to2}^* \frac{dx_2}{dt}\rangle] = (1/2)Im[\kappa_{12}\omega\langle x_1^* x_2\rangle]$. The fluctuating forces have the form of $\langle F_i^*(\omega')F_j(\omega)\rangle = 8\pi m\gamma\Theta(\omega,T_j)\delta(\omega-\omega')\delta_{ij}, (i,j=1,2)$.

B. Derivation of the coupled mode theory for the harmonic oscillator model

Having derived the heat transfer properties between two harmonic oscillators at different temperatures, we now seek to describe the same system with the coupled mode theory formalism. While the harmonic oscillators above are described with a second-order differential equation, the coupled mode theory equation used in Refs. 42 and 43 involves only a first-order derivative in time. We therefore assume that

$$x_{1,2}(t) = \frac{\tilde{x}_{1,2}(t)e^{-i\omega t} + \tilde{x}_{1,2}^*(t)e^{i\omega t}}{2}, \tag{20}$$

$$F_{1,2}(t) = \frac{\tilde{F}_{1,2}(t)e^{-i\omega t} + \tilde{F}^*_{1,2}(t)e^{i\omega t}}{2}, \tag{21}$$

and apply the slowly varying envelope approximation, which is valid in the regime $\omega \gg \gamma$. Substituting Eqs. (20) and (21) into Eq. (17) and selecting the $\exp(-i\omega t)$ term, we have

$$\frac{d^2}{dt^2}\begin{pmatrix}\tilde{x}_1\\ \tilde{x}_2\end{pmatrix} + (\gamma - i2\omega)\frac{d}{dt}\begin{pmatrix}\tilde{x}_1\\ \tilde{x}_2\end{pmatrix} + \begin{pmatrix}\frac{\omega_H^2+\omega_L^2}{2} - \omega^2 - i\gamma\omega & -\frac{\omega_H^2-\omega_L^2}{2}\\ -\frac{\omega_H^2-\omega_L^2}{2} & \frac{\omega_H^2+\omega_L^2}{2} - \omega^2 - i\gamma\omega\end{pmatrix}\begin{pmatrix}\tilde{x}_1\\ \tilde{x}_2\end{pmatrix} = \frac{1}{m}\begin{pmatrix}\tilde{F}_1\\ \tilde{F}_2\end{pmatrix}. \tag{22}$$

We ignore the second-order derivative and use approximations of $[\omega^2 - (\omega_H^2 + \omega_L^2)/2]/(2\omega) \approx \omega - (\omega_H + \omega_L)/2$ for the modal frequency term and $(\omega_H^2 - \omega_L^2)/(4\omega) \approx (\omega_H - \omega_L)/2$ for the coupling term. As a result, we arrive at the coupled mode equation, and the formula for power transfer, respectively, as

$$\frac{d}{dt}\begin{pmatrix}\tilde{x}_1\\ \tilde{x}_2\end{pmatrix} + \begin{pmatrix}i\frac{\omega_H+\omega_L}{2} + \frac{\gamma}{2} & -i\frac{\omega_H-\omega_L}{2}\\ -i\frac{\omega_H-\omega_L}{2} & i\frac{\omega_H+\omega_L}{2} + \frac{\gamma}{2}\end{pmatrix}\begin{pmatrix}\tilde{x}_1\\ \tilde{x}_2\end{pmatrix} = i\frac{1}{m(\omega_H+\omega_L)}\begin{pmatrix}\tilde{F}_1\\ \tilde{F}_2\end{pmatrix}, \tag{23}$$

$$\begin{aligned} P_{1\to 2} &= Re\left[\left\langle F^*{}_{1\to 2}\frac{dx_2}{dt}\right\rangle\right] \\ &= \frac{1}{2}Im\left[m\frac{\omega_H^2-\omega_L^2}{2}\int_{-\infty}^{\infty}\frac{d\omega}{2\pi}\int_{-\infty}^{\infty}\frac{d\omega'}{2\pi}e^{-i(\omega-\omega')t}\frac{\omega_H+\omega_L}{2}\langle\tilde{x}_1^*(\omega')\tilde{x}_2(\omega)\rangle\right] \\ &= \int_{-\infty}^{\infty}\frac{d\omega}{2\pi}\frac{4\left(\frac{\gamma}{2}\right)^2\left(\frac{\omega_H-\omega_L}{2}\right)^2[\Theta(\omega,T_1)-\Theta(\omega,T_2)]}{\left|\left[-i\left(\omega-\frac{\omega_H+\omega_L}{2}\right)+\frac{\gamma}{2}\right]^2+\left(\frac{\omega_H-\omega_L}{2}\right)^2\right|^2}, \end{aligned} \tag{24}$$

where we have used $\tilde{F}_i(\omega) = 16\pi m\gamma\Theta(\omega, T_i)\delta(\omega - \omega')$, $(i = 1, 2)$ that comes from the derivation process of Eqs. (1)–(10) with Eqs. (20) and (21). Eq. (24) agrees with Eq. (19) in the proper limit.

Eq. (23) provides a coupled mode theory description of the physical system as discussed in Section II A. We emphasize that in the coupled mode theory formalism, the modal frequency for the "individual" mode is $(\omega_H + \omega_L)/2$, which is different from the resonant frequency of an independent harmonic oscillator $\omega_s = \sqrt{\kappa/m}$. To describe this system with the coupled mode theory, one must take into account the frequency shift of an oscillator due to the presence of the other oscillator, which was not included in Refs. 42 and 43. On the other hand, the coupling constant $(\omega_H - \omega_L)/2$ in our coupled mode theory is the same as in Refs. 42 and 43.

III. COMPARISON OF THEORY TO NUMERICAL RESULTS

We compare our coupled mode theory results (Eq. (24)) to results from fluctuational electrodynamics calculation in the near-field heat transfer between SiC plates (inset of Fig. 2) in Section III A and between graphene layers (inset of Fig. 4) in Section III B. We assume identical bodies with temperatures $T_1 = T + \Delta T$ and $T_2 = T$ placed with a vacuum gap size of $d = 10$ nm and investigate the temperature derivative of heat transfer per channel at $T = 300$ K. In Section III C, we extend our formalism to the near-field heat transfer in a four-layer graphene structure and verify the applicability of the formalism by comparing the analytical results to the numerical results.

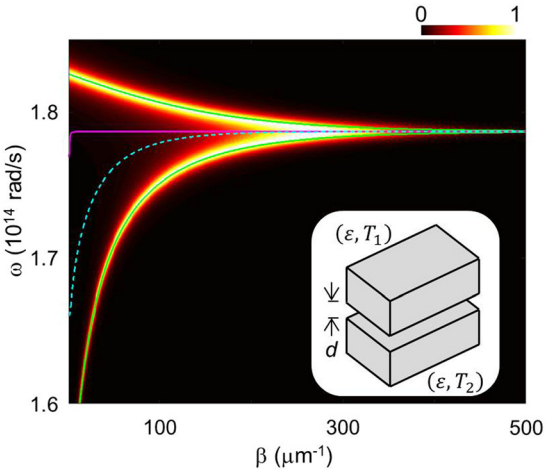

FIG. 2. Normalized exchange function $Z(\omega, \beta)$ defined in Eq. (26) in the SiC plate-plate structure with temperatures $T_1 = T + \Delta T$ and $T_2 = T$. Dispersion curves ω_H and ω_L are obtained from Eq. (28) and plotted by the green solid lines. The average of ω_H and ω_L (cyan dashed line) and the dispersion curve ω_s (pink solid line) of a single SiC plate (Eq. (29)) are presented. Parameters are $d = 10$ nm and $T = 300$ K.

In all three cases considered here, the p-polarized evanescent waves dominantly contribute to the heat transfer in the near-field regime, since the surface plasmon or phonon polaritons are p-polarized. The heat transfer is treated as a summation of independent channels indexed by the lateral wavenumber β[29,35,42,43] and the net heat flux is given by[15]

$$\Phi = \int_{k_0}^{\infty} \frac{\beta d\beta}{2\pi} \Phi_c(\beta), \tag{25}$$

where the heat transfer per channel is defined as

$$\begin{aligned}\Phi_c(\beta) &= \int_0^{\infty} \frac{d\omega}{2\pi} Z(\omega,\beta)[\Theta(\omega,T_1) - \Theta(\omega,T_2)] \\ &= \int_0^{\infty} \frac{d\omega}{2\pi} \frac{4\{Im[r(\omega,\beta)]\}^2 e^{-2\kappa_0 d}}{|1 - r(\omega,\beta)^2 e^{-2\kappa_0 d}|^2} \\ &\quad \times [\Theta(\omega,T_1) - \Theta(\omega,T_2)].\end{aligned} \tag{26}$$

In Eq. (26), the exchange function Z satisfies $0 \le Z \le 1$. $r(\omega,\beta)$ is the Fresnel reflection coefficient of the p-polarized evanescent waves at the body-vacuum interface. κ_0 is the normal wavenumber in vacuum and has the form of $\kappa_0 = \sqrt{\beta^2 - k_0^2}$ $(k_0 < \beta)$, where k_0 is the free space wavenumber.

A. SiC case

The behavior of the exchange function Z can be well understood by analyzing the dispersion relation of parallel surfaces. Here we consider the heat transfer between SiC plates (inset of Fig. 2). The permittivity of SiC is expressed as

$$\varepsilon(\omega) = \varepsilon_\infty \left(1 + \frac{\omega_{LO}^2 - \omega_{TO}^2}{\omega_{TO}^2 - \omega^2 - i\gamma\omega}\right), \tag{27}$$

where $\omega_{LO} = 969\,\mathrm{cm}^{-1}$, $\omega_{TO} = 793\,\mathrm{cm}^{-1}$, $\gamma = 4.76\,\mathrm{cm}^{-1}$, and $\varepsilon_\infty = 6.7$.[14] The exchange function $Z(\omega,\beta)$ is calculated by plugging the Fresnel reflection coefficient $r(\omega,\beta) = [\varepsilon(\omega)\kappa_0 - \kappa]/[\varepsilon(\omega)\kappa_0 + \kappa]$, where $\kappa = \sqrt{\beta^2 - \varepsilon k_0^2}$, into Eq. (26), and shown in Fig. 2. To apply the coupled mode theory to heat transfer, we determine the dispersion relation of the plate-plate structure by solving the dispersion equation

$$\left(\frac{\varepsilon(\omega)}{\kappa} + \frac{1}{\kappa_0}\right)^2 e^{\kappa_0 d} - \left(\frac{\varepsilon(\omega)}{\kappa} - \frac{1}{\kappa_0}\right)^2 e^{-\kappa_0 d} = 0, \tag{28}$$

with a real β and complex ω.[46] The real part of ω is plotted in Fig. 2 as the green solid lines. At each β, there are two solutions labelled as ω_H and ω_L. We see that in the ω-β plane the exchange function Z reaches near unity (white-color regions) only in the vicinity of the dispersion relation $\omega_H(\beta)$ and $\omega_L(\beta)$. Therefore, one can describe the near-field heat transfer between parallel surfaces with two frequencies ω_H and ω_L in the system.

The heat transfer per channel between SiC plates is analytically and numerically investigated for different β s, and plotted in Fig. 3(a) together with three spectra at $\beta = 20\,\mu\mathrm{m}^{-1}$, $200\,\mu\mathrm{m}^{-1}$, and $500\,\mu\mathrm{m}^{-1}$ in Figs. 3(b)–3(d). In the spectra of

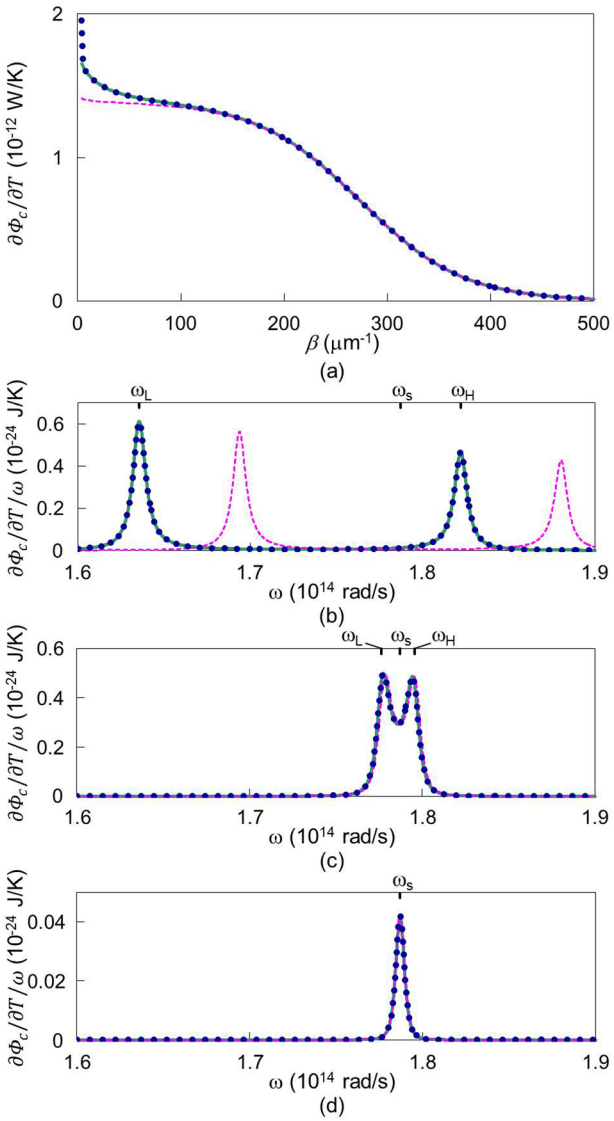

FIG. 3. (a) Heat transfer per channel as a function of β and the spectra at (b) $\beta = 20\,\mu\mathrm{m}^{-1}$, (c) $\beta = 200\mu\mathrm{m}^{-1}$, and (d) $\beta = 500\,\mu\mathrm{m}^{-1}$ in the SiC case [green solid lines: coupled mode theory, Eq. (24), pink dashed lines: coupled mode theory with ω_s instead of $(\omega_H + \omega_L)/2$ in Eq. (24), blue dots: fluctuational electrodynamics, Eq. (26)].

Figs. 3(b)–3(d), as β increases, two resonant peaks approach each other and eventually merge as a single peak and the amplitude of the single peak then decreases as β is increased beyond the cut-off wavenumber $\beta_c \approx 280\,\mu\mathrm{m}^{-1}$. The analytical theory (green solid line, Eq. (24)) excellently agrees with numerical results (blue dots, Eq. (26)) over the entire range of wavevectors.

For comparison, we calculate the heat transfer per channel by using the conventional coupled mode theory of Refs. 42 and 43, where the modal frequency is characterized by the polariton frequency $\omega_s(\beta)$ of a single SiC-vacuum interface; thus, the heat transfer per channel takes the form $P_{1\to2} = \int_0^{\infty} \frac{d\omega}{2\pi} \frac{4\left(\frac{\gamma}{2}\right)^2 \left(\frac{\omega_H - \omega_L}{2}\right)^2 [\Theta(\omega,T_1) - \Theta(\omega,T_2)]}{\left|\left[-i(\omega-\omega_s) + \frac{\gamma}{2}\right]^2 + \left(\frac{\omega_H - \omega_L}{2}\right)^2\right|^2}$ and is plotted as the pink dashed lines in Figure 3. The frequency ω_s (pink solid line) has been obtained from the dispersion equation of a single interface

$$\frac{\varepsilon(\omega)}{\kappa}+\frac{1}{\kappa_0}=0. \tag{29}$$

The conventional theory agrees well with numerical results in the quasi-static regime (Figs. 3(c) and 3(d)). However, when $\beta \leq 100\,\mu\text{m}^{-1}$, discrepancy between the conventional theory (pink dashed line) and the exact results (blue dots) becomes substantial as shown in Figs. 3(a) and 3(b). This can be understood from the comparison of dispersion curves in Fig. 2. The dispersion curve of ω_s (pink solid line) gets far away from $(\omega_H+\omega_L)/2$ (cyan dashed line) as β decreases from $100\,\mu\text{m}^{-1}$. The comparison above clearly indicates the importance of including the frequency shift in order to correctly treat the heat transfer in the coupled mode theory.

B. Two-layer graphene case

In the graphene case (inset of Fig. 4), the optical conductivity of graphene, including both the Drude and interband contributions, is expressed as[47]

$$\sigma = i\frac{2e^2k_BT}{\pi\hbar^2(\omega+i\gamma)}ln\left[2\cos h\left(\frac{\mu}{2k_BT}\right)\right] + \frac{e^2}{4\hbar}\left[G\left(\frac{\hbar\omega}{2}\right)+i\frac{4\hbar\omega}{\pi}\int_0^\infty\frac{G(\xi)-G\left(\frac{\hbar\omega}{2}\right)}{(\hbar\omega)^2-4\xi^2}d\xi\right], \tag{30}$$

where $G(\xi)=\sin h(\xi/k_BT)/[\cos h(\mu/k_BT)+\cos h(\xi/k_BT)]$. We assume a damping rate of $\gamma=10^{13}\,\text{rad/s}$ for graphene.[19–21] The chemical potential of graphene is set at $\mu=0.3\,\text{eV}$. The exchange function Z is obtained via the Fresnel reflection coefficient $r(\omega,\beta)=[1-i2\varepsilon_0\omega/(\sigma\kappa_0)]^{-1}$ and shown in Fig. 4. Similar to the SiC case, the peaks of the exchange function Z agree well with the dispersion relation $\omega_H(\beta)$ and $\omega_L(\beta)$ obtained by solving the dispersion equation[19]

$$\left(\frac{2}{\kappa_0}+i\frac{\sigma}{\varepsilon_0\omega}\right)^2e^{\kappa_0 d}+\left(\frac{\sigma}{\varepsilon_0\omega}\right)^2e^{-\kappa_0 d}=0. \tag{31}$$

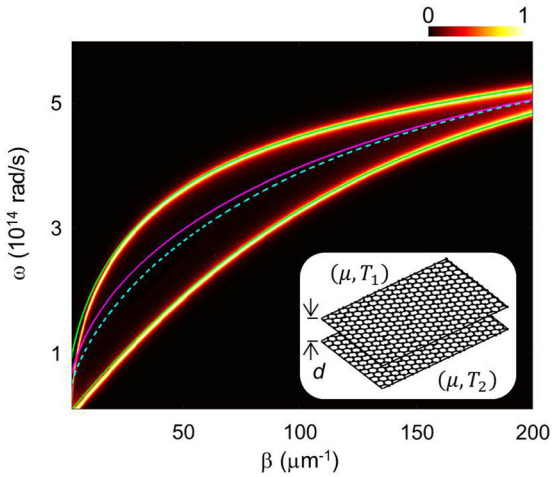

FIG. 4. Normalized exchange function $Z(\omega,\beta)$ in the two-layer graphene structure with temperatures $T_1=T+\Delta T$ and $T_2=T$. Dispersion curves ω_H and ω_L are obtained from Eq. (31) and plotted by the green solid lines. The average of ω_H and ω_L (cyan dashed line) and the dispersion curve ω_s (pink solid line) of a single graphene layer (Eq. (32)) are presented. Parameters are $d=10\,\text{nm}$, $T=300\,\text{K}$, and $\mu=0.3\,\text{eV}$.

The heat transfer per channel between graphene layers as a function of wavenumber β and three heat transfer spectra at $\beta=5\,\mu\text{m}^{-1}$, $25\,\mu\text{m}^{-1}$, and $100\,\mu\text{m}^{-1}$ are shown in Figs. 5(a)–5(d). The coupled mode theory results (green solid line, Eq. (24)) agree excellently with numerical results (blue dots, Eq. (26)). In the spectra of Figs. 5(b)–5(d), as β increases, ω_H and ω_L increase as can be seen from the dispersion curves (green solid lines) of Fig. 4. Since $\Theta(\omega,T)$ decreases as a function of ω, the heat transfer per channel decreases with the increase of β (Fig. 5(a)), and moreover, at each β the heat transfer is dominated by the peak at the lower resonant frequency ω_L (Figs. 5(b)–5(d)).

We plot the dispersion curve of the polariton frequency ω_s of a single graphene layer, which is obtained from Eq. (32), in Fig. 4 as the pink solid line

$$\frac{2}{\kappa_0}+i\frac{\sigma}{\varepsilon_0\omega}=0. \tag{32}$$

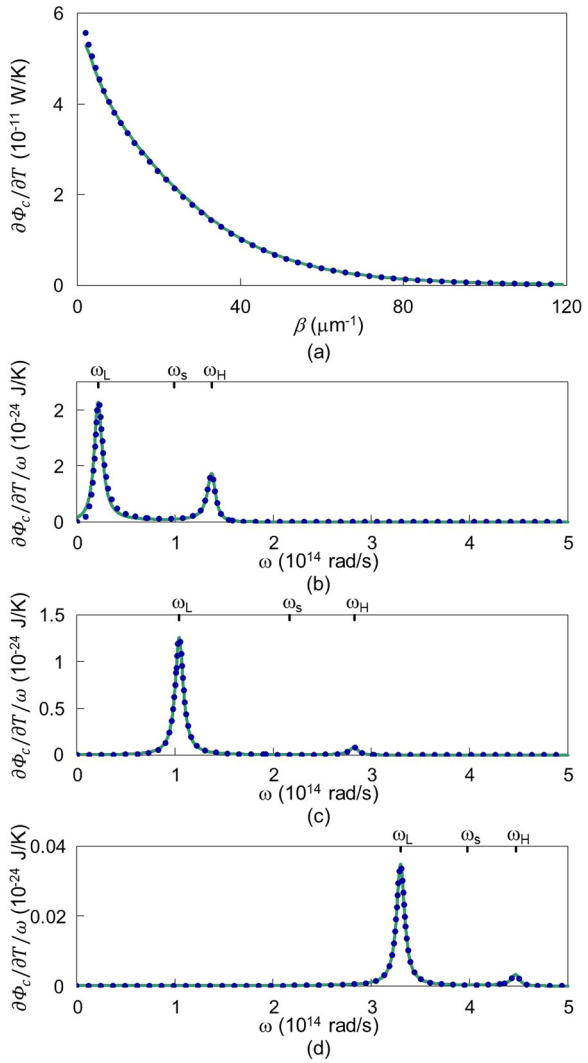

FIG. 5. (a) Heat transfer per channel as a function of β and the spectra at (b) $\beta=5\,\mu\text{m}^{-1}$, (c) $\beta=25\,\mu\text{m}^{-1}$, and (d) $\beta=100\,\mu\text{m}^{-1}$ in the graphene case [green solid lines: coupled mode theory, Eq. (24), blue dots: fluctuational electrodynamics, Eq. (26)].

We see $\omega_s > (\omega_H + \omega_L)/2$ over most of wavevectors that contribute to the heat transfer. Therefore, in the graphene case, including the frequency shift in the coupled mode theory is even more important as compared to the SiC case.

C. Four-layer graphene case

Our theory is not limited to systems where the heat transfer is carried by two resonant modes, and instead can be applied to more complex situations. As an illustration, here, we consider near-field heat transfer in a structure consisting of four identical graphene layers, where the top two layers and the bottom two layers have temperatures of $T_H = T + \Delta T$ and $T_L = T$, respectively (the inset of Fig. 6(a)). The reflection coefficient of the two layers of graphene from the vacuum gap is given by

$$\tilde{r} = r + \frac{t^2 r e^{-2\kappa_0 l}}{1 - r^2 e^{-2\kappa_0 l}}, \tag{33}$$

where $r = [1 - i2\varepsilon_0\omega/(\sigma\kappa_0)]^{-1}$ and $t = -i2\varepsilon_0\omega/(\sigma\kappa_0)[1 - i2\varepsilon_0\omega/(\sigma\kappa_0)]^{-1}$. The exchange function Z for the four-layer case is obtained from Eqs. (26) and (33), and shown in Fig. 6(a). Similar to the cases considered above, at each β the exchange function Z exhibits four peaks. The positions of these peaks agree well with the dispersion relation $\omega_{c1}(\beta)$, $\omega_{c2}(\beta)$, $\omega_{c3}(\beta)$, and $\omega_{c4}(\beta)$ obtained by solving the dispersion equation

$$\left[\left(\frac{2}{\kappa_0} + i\frac{\sigma}{\varepsilon_0\omega}\right)^2 e^{\kappa_0 l} + \left(\frac{\sigma}{\varepsilon_0\omega}\right)^2 e^{-\kappa_0 l}\right]^2 e^{\kappa_0 d} + \left(\frac{\sigma}{\varepsilon_0\omega}\right)^2 \left[\left(\frac{2}{\kappa_0} + i\frac{\sigma}{\varepsilon_0\omega}\right) e^{\kappa_0 l} + \left(\frac{2}{\kappa_0} - i\frac{\sigma}{\varepsilon_0\omega}\right) e^{-\kappa_0 l}\right]^2 e^{-\kappa_0 d} = 0. \tag{34}$$

In order to describe the system in the coupled mode theory formalism, we assume that there exists only the nearest coupling between graphene layers and that the inner layers and the outer layers have different modal frequencies induced by the coupling effect. Following the derivation process in Section II, that is, applying the slowly varying envelope approximation to the equations of motion for the symmetric model system of the four oscillators coupled together, as shown in Fig. 6(b), we have the coupled mode equation that involves a first-order derivative in time as:

$$\frac{d}{dt}\begin{pmatrix} \tilde{x}_1 \\ \tilde{x}_2 \\ \tilde{x}_3 \\ \tilde{x}_4 \end{pmatrix} + \begin{pmatrix} i\omega_1 + \frac{\gamma}{2} & -i\kappa_{12} & 0 & 0 \\ -i\kappa_{12} & i\omega_2 + \frac{\gamma}{2} & -i\kappa_{23} & 0 \\ 0 & -i\kappa_{23} & i\omega_2 + \frac{\gamma}{2} & -i\kappa_{12} \\ 0 & 0 & -i\kappa_{12} & i\omega_1 + \frac{\gamma}{2} \end{pmatrix} \begin{pmatrix} \tilde{x}_1 \\ \tilde{x}_2 \\ \tilde{x}_3 \\ \tilde{x}_4 \end{pmatrix} = i\frac{2}{m(\omega_{c1} + \omega_{c2} + \omega_{c3} + \omega_{c4})} \begin{pmatrix} \tilde{F}_1 \\ \tilde{F}_2 \\ \tilde{F}_3 \\ \tilde{F}_4 \end{pmatrix}, \tag{35}$$

where

$$\omega_1 = \frac{\omega_{c1} + \omega_{c2} + \omega_{c3} + \omega_{c4}}{4} - \Delta\omega_c, \tag{36}$$

$$\omega_2 = \frac{\omega_{c1} + \omega_{c2} + \omega_{c3} + \omega_{c4}}{4} + \Delta\omega_c, \tag{37}$$

$$\kappa_{12} = \sqrt{\frac{\omega_{c2}\omega_{c4}(\omega_{c1} + \omega_{c3}) - \omega_{c1}\omega_{c3}(\omega_{c2} + \omega_{c4})}{(\omega_{c2} + \omega_{c4}) - (\omega_{c1} + \omega_{c3})} - \left[\frac{\omega_{c2}\omega_{c4} - \omega_{c1}\omega_{c3}}{(\omega_{c2} + \omega_{c4}) - (\omega_{c1} + \omega_{c3})}\right]^2}, \tag{38}$$

$$\kappa_{23} = \frac{(\omega_{c2} + \omega_{c4}) - (\omega_{c1} + \omega_{c3})}{2}, \tag{39}$$

$$\Delta\omega_c = \frac{\omega_{c1} + \omega_{c2} + \omega_{c3} + \omega_{c4}}{4} - \frac{\omega_{c2}\omega_{c4} - \omega_{c1}\omega_{c3}}{(\omega_{c2} + \omega_{c4}) - (\omega_{c1} + \omega_{c3})}. \tag{40}$$

Eqs. (36)–(40) are derived such that the resonant frequencies of Eq. (35) match those of the dispersion relation of the four-layer graphene structure. We observe in Eqs. (36) and (37) that the frequency of the individual mode for the outer two layers is shifted down by $\Delta\omega_c$ from the average of the four frequencies $(\omega_{c1} + \omega_{c2} + \omega_{c3} + \omega_{c4})/4$, whereas the frequency of the individual mode for the inner two layers is shifted up by $\Delta\omega_c$. In Figure 6(a), we compare the frequencies of the individual modes (cyan dashed lines) with the dispersion relation of the four-layer structure (green solid lines) and the dispersion relation of the two-layer forming one of the bodies (pink solid lines). We clearly see that the frequencies of the individual modes are different from the dispersion relation of the two-layer system.

The near-field heat transfer from the hot graphene layers to the cold graphene layers is described by the power transfer $P_{2\to3} = Re[\langle F^*_{2\to3}\frac{dx_3}{dt}\rangle] \approx Im[m\kappa_{23}(\frac{\omega_{c1}+\omega_{c2}+\omega_{c3}+\omega_{c4}}{4})^2\langle\tilde{x}^*_2\tilde{x}_3\rangle]$ in the harmonic oscillator model. The formula for the power transfer is finally derived as

$$P_{2\to3} = \int_0^\infty \frac{d\omega}{2\pi} \frac{4\left(\frac{\gamma}{2}\right)^2\kappa_{23}^2\left[\left|-i(\omega-\omega_1)+\frac{\gamma}{2}\right|^2+\kappa_{12}^2\right]^2[\Theta(\omega,T_H)-\Theta(\omega,T_L)]}{\left|\left[-i(\omega-\omega_{c1})+\frac{\gamma}{2}\right]\left[-i(\omega-\omega_{c2})+\frac{\gamma}{2}\right]\left[-i(\omega-\omega_{c3})+\frac{\gamma}{2}\right]\left[-i(\omega-\omega_{c4})+\frac{\gamma}{2}\right]\right|^2}. \quad (41)$$

The analytical result and the numerical result of the power transfer are obtained from Eq. (41) with the four frequencies (green solid lines) in Fig. 6(a) and from Eq. (26) with $Z(\omega,\beta)$ in Fig. 6(a), respectively. The analytical result (green solid line) excellently agrees with the numerical result (blue dots) in the heat transfer per channel at $\beta = 25\,\mu\text{m}^{-1}$ in Fig. 6(c).

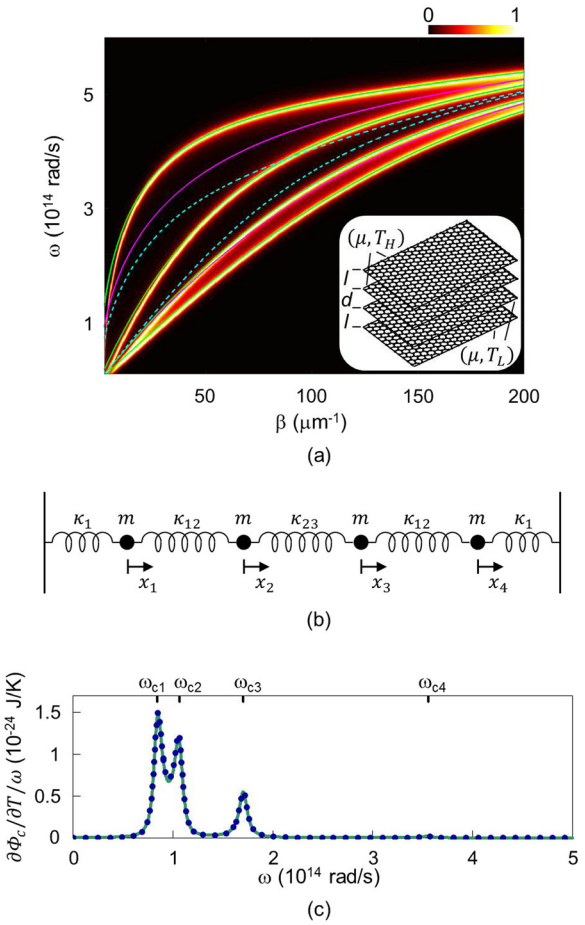

FIG. 6. (a) Normalized exchange function $Z(\omega,\beta)$ in the four-layer graphene structure (inset). The top two layers and the bottom two layers have temperatures of $T_H = T + \Delta T$ and $T_L = T$, respectively. Parameters are $d = l = 10\,\text{nm}$, $T = 300\,\text{K}$, and $\mu = 0.3\,\text{eV}$. Four dispersion curves are obtained from Eq. (34) and plotted by the green solid lines. The frequencies of the individual modes for the outer two layers (Eq. (36)) and the inner two layers (Eq. (37)) are plotted by the cyan dashed lines. The dispersion curves of the two-layer forming one of the bodies (pink solid lines, which are the same as the green solid lines in Fig. 4) are presented for comparison. (b) Analytic model of four-coupled harmonic oscillators. (c) Spectral heat transfer per channel at $\beta = 25\,\mu\text{m}^{-1}$ [green solid line: coupled mode theory, Eq. (41), blue dots: fluctuational electrodynamics, Eq. (26)].

IV. CONCLUSION

We have explored the coupled mode theory for near-field heat transfer between parallel surfaces. We have established a coupled mode equation by using a harmonic oscillator model and then derived the coupled mode theory formalism by introducing a slowly varying envelop approximation. In our formalism, the heat transfer is linked to the dispersion relation of the coupled system with ω_H and ω_L, and therefore, the frequency shift $\omega_s - (\omega_H + \omega_L)/2$ as induced by the second interface is included. Our results have revealed that the coupled mode theory formalism completely accounts for exact numerical results over all range of wavevectors in heat transfer between SiC plates and between graphene layers. In addition, we have applied our formalism to the near-field heat transfer in a four-layer structure of graphene and demonstrated that the coupled mode theory formalism can be successfully applied in systems where more than two modes contribute to the heat transfer. Our results show that near-field heat transfer can be quantitatively accounted for by the study of the underlying electromagnetic modes. And therefore, the control of these modes may lead to the control of heat transfer.

ACKNOWLEDGMENTS

Professor Fan's contribution to this publication was as a consultant, and was not part of his Stanford duties or responsibilities.

[1]D. Polder and M. Van Hove, Phys. Rev. B **4**, 3303 (1971).
[2]D. G. Calhill, P. V. Braun, G. Chen, D. R. Clarke, S. Fan, K. E. Goodson, P. Keblinski, W. P. King, G. D. Mahan, A. Majumdar, H. J. Maris, S. R. Phillspot, E. Pop, and L. Shi, Appl. Phys. Rev. **1**, 011305 (2014).
[3]E. Rousseau, A. Siria, G. Jourdan, S. Volz, F. Comin, J. Chevrier, and J.-J. Greffet, Nat. Photonics **3**, 514 (2009).
[4]S. Shen, A. Narayanaswamy, and G. Chen, Nano Lett. **9**, 2909 (2009).
[5]K. Kim, B. Song, V. Fernandez-Hurtado, W. Lee, W. Jeong, L. Cui, D. Thompson, J. Feist, M. T. Homer Reid, F. J. Garcia-Vidal, J. C. Cuevas, E. Meyhofer, and P. Reddy, Nature **528**, 387 (2015).
[6]L. Hu, A. Narayanaswamy, X. Chen, and G. Chen, Appl. Phys. Lett. **92**, 133106 (2008).
[7]R. S. Ottens, V. Quetschke, S. Wise, A. A. Alemi, R. Lundock, G. Mueller, D. H. Reitze, D. B. Tanner, and B. F. Whiting, Phys. Rev. Lett. **107**, 014301 (2011).
[8]R. St-Gelais, B. Guha, L. Zhu, S. Fan, and M. Lipson, Nano Lett. **14**, 6971 (2014).
[9]K. Ito, A. Miura, H. Iizuka, and H. Toshiyoshi, Appl. Phys. Lett. **106**, 083504 (2015).

[10]B. Guha, C. Otey, C. B. Poitras, S. Fan, and M. Lipson, Nano Lett. **12**, 4546 (2012).
[11]A. Kittel, W. Muller-Hirsch, J. Parisi, S.-A. Biehs, D. Reddig, and M. Holthaus, Phys. Rev. Lett. **95**, 224301 (2005).
[12]Y. De Wilde, F. Formanek, R. Carminati, B. Gralak, P.-A. Lemoine, K. Joulain, J.-P. Mulet, Y. Chen, and J.-J. Greffet, Nature **444**, 740 (2006).
[13]A. C. Jones and M. B. Raschke, Nano Lett. **12**, 1475 (2012).
[14]K. Joulain, J.-P. Mulet, F. Marquier, R. Carminati, and J.-J. Greffet, Surf. Sci. Rep. **57**, 59 (2005).
[15]S. Basu, Z. M. Zhang, and C. J. Fu, Int. J. Energy Res. **33**, 1203–1232 (2009).
[16]C. R. Otey, L. Zhu, S. Sandhu, and S. Fan, J. Quant. Spectrosc. Radiat. Transfer **132**, 3 (2014).
[17]S.-A. Biehs, P. Ben-Abdallah, F. S. S. Rosa, K. Joulain, and J.-J. Greffet, Opt. Express **19**, A1088 (2011).
[18]S.-A. Biehs, M. Tschikin, and P. Ben-Abdallah, Phys. Rev. Lett. **109**, 104301 (2012).
[19]O. Ilic, M. Jablan, J. D. Joannopoulos, I. Celanovic, H. Buljan, and M. Soljacic, Phys. Rev. B **85**, 155422 (2012).
[20]V. B. Svetovoy, P. J. van Zwol, and J. Chevrier, Phys. Rev. B **85**, 155418 (2012).
[21]X. Liu, R. Z. Zhang, and Z. M. Zhang, ACS Photonics **1**, 785 (2014).
[22]A. Narayanaswamy and G. Chen, Phys. Rev. B **77**, 075125 (2008).
[23]C. Otey and S. Fan, Phys. Rev. B **84**, 245431 (2011).
[24]M. Kruger, T. Emig, and M. Kardar, Phys. Rev. Lett. **106**, 210404 (2011).
[25]S. Basu and M. Francoeur, Appl. Phys. Lett. **98**, 113106 (2011).
[26]H. Iizuka and S. Fan, J. Appl. Phys. **112**, 024304 (2012).
[27]P. Ben-Abdallah and S.-A. Biehs, Phys. Rev. Lett. **112**, 044301 (2014).
[28]V. Kubytskyi, S.-A. Biehs, and P. Ben-Abdallah, Phys. Rev. Lett. **113**, 074301 (2014).
[29]J. B. Pendry, J. Phys.: Condens. Matter **11**, 6621 (1999).
[30]A. I. Volokitin and B. N. J. Persson, Phys. Rev. B **69**, 045417 (2004).
[31]S. Basu and Z. M. Zhang, J. Appl. Phys. **105**, 093535 (2009).
[32]P. Ben-Abdallah and K. Joulain, Phys. Rev. B **82**, 121419(R) (2010).
[33]S.-A. Biehs, E. Rousseau, and J.-J. Greffet, Phys. Rev. Lett. **105**, 234301 (2010).
[34]P. Rodriguez-Lopez, W.-K. Tse, and D. A. R. Dalvit, J. Phys.: Condens. Matter **27**, 214019 (2015).
[35]H. Iizuka and S. Fan, Phys. Rev. B **92**, 144307 (2015).
[36]H. A. Haus, *Waves and Fields in Optoelectronics* (Prentice-Hall, Englewood Cliffs, NJ, 1984).
[37]H. A. Haus, W. P. Huang, S. Kawakami, and N. A. Whitaker, J. Lightwave Technol. **5**, 16 (1987).
[38]H. A. Haus and W. P. Huang, Proc. IEEE **79**, 1505 (1991).
[39]C. Manolatou, M. J. Khan, S. Fan, P. R. Villeneuve, H. A. Haus, and J. D. Joannopoulos, IEEE J. Quantum Electron. **35**, 1322 (1999).
[40]S. Fan, W. Suh, and J. D. Joannopoulos, J. Opt. Soc. Am. A **20**, 569 (2003).
[41]M. F. Yanik and S. Fan, Phys. Rev. Lett. **92**, 083901 (2004).
[42]C. R. Otey, W. T. Lau, and S. Fan, Phys. Rev. Lett. **104**, 154301 (2010).
[43]H. Chalabi, E. Hasman, and M. L. Brongersma, Opt. Express **22**, 30032 (2014).
[44]M. Francoeur, M. P. Menguc, and R. Vaillon, J. Appl. Phys. **107**, 034313 (2010).
[45]M. Francoeur, M. P. Menguc, and R. Vaillon, J. Phys. D: Appl. Phys. **43**, 075501 (2010).
[46]A. Archambault, M. Besbes, and J.-J. Greffet, Phys. Rev. Lett. **109**, 097405 (2012).
[47]L. A. Falkovsky, J. Phys.: Conf. Ser. **129**, 012004 (2008).